Agricultural and Forest Meteorology 263 (2018) 399–408

Contents lists available at ScienceDirect

Agricultural and Forest Meteorology

journal homepage: www.elsevier.com/locate/agrformet

Correction of anisotropy effects on penta-needle heat-pulse probe sap-flux density and thermal property measurements

Sheng Wang[a,b,c], Jun Fan[a,b,*], Scott B. Jones[d]

[a] State Key Laboratory of Soil Erosion and Dryland Farming on the Loess Plateau, Northwest A&F University, No.3 Taicheng Road, Yangling 712100, Shaanxi, China
[b] Institute of Soil and Water Conservation, Chinese Academy of Sciences and Ministry of Water Resources, No. 26 Xinong Road, Yangling 712100, Shaanxi, China
[c] University of Chinese Academy of Sciences, No. 19 (A) Yuquan Road, Shijingshan District, Beijing 100049, China
[d] Department of Plants, Soils and Climate, Utah State University, Logan, UT 84322, USA

ARTICLE INFO

Keywords:
Sap flow
Thermal properties
Wood water content
INV-WATFLX
Heat pulse
PHPP
Anisotropy

ABSTRACT

Growing interest in methods for estimating plant stem/trunk sap-flux density and thermal properties include the use of heated needles inserted into the plant. A penta-needle heat-pulse probe (PHPP) coupled with an on-chip integrated INV-WATFLX algorithm was newly developed for inverse estimation of isotropic porous media thermal-diffusivity, κ, -conductivity, λ, and heat velocity, V_h (converted to water-flux density, J), thus heat capacity, C (=λ/κ), and water content could also be derived. This integrated sensor, however, has yet to be applied in anisotropic sapwood sensing. Here, we conducted a numerical simulation of the PHPP heat pulse and a deviation analysis when using an INV-WATFLX code developed by Yang and Jones [Comput. Geosci.—UK. 35 (2009) 2250] in anisotropic porous media. Deviations in J were up to +40% and as low as -30%, and within 12% in κ, λ and C at static conditions for varied PHPP installation angles, α, in sapwood. We developed a correction of anisotropy effects, and followed up with a field test of the sensors installed on standing poplar (*Populus simonii* Carr.) trees using $\alpha = 0^\circ$, 15° and 30°. Field tests showed the corrected J estimated using PHPPs at $\alpha = 15^\circ$ and 30° both agreed well with J from thermal dissipation probes (TDPs) in 1:1 line ($R^2 = 0.87$ and 0.83, $P < 0.01$). The corrected J at $\alpha = 0^\circ$ showed an apparent 30% underestimate ($R^2 = 0.87$, $P < 0.01$), which was assumed to be due to wound effects. All PHPP estimates exhibited similar and stable κ, λ and C at night, but showed a diurnal fluctuation in J to varying extents likely due to the flow turbulence by inserted needles.

1. Introduction

Sap flow measurement facilitates a unique and practical tool for investigating whole-plant transpiration and plant-water relations (David et al., 2013). It is of growing interest in advancing techniques for accurately estimating sap flow and stem thermal properties by using the heated needles inserted into plant xylem. These techniques derive sap flow via tracing the heat transported through the mobile sap, by injecting an exogenous heat source and measuring the resulting changes in temperature field around the heater. The family of current sap flow techniques mainly comprises the continuous heating based heat balance, thermal dissipation probe (TDP) and heat field deformation methods, and a wide range of heat pulse (HP) methods. Within them, most of current HP techniques – including compensation heat pulse velocity (CHP), Tmax and heat ratio (HR) methods – quantify sap-flux density (J) by measuring the velocity of heat (V_h) introduced into sapwood; Tmax method can also resolve thermal diffusivity (κ) from the recorded travel time for the temperatures to peak, t_m, in the upright temperature needle. They originate from a widespread analytical solution of the fundamental heat convection-conduction equation on an assumption of instantaneous infinite line source of heat (IILS) in isotropic media given by Marshall (1958). In practice, however, they apply a pulsed infinite line source of heat (PILS) with heating durations up to 10 s, rather than the relatively small heating duration (0.25–1.5 s) used by Cohen et al. (1981), to relieve the possible excessive heating damage to plant at heater position. Kluitenberg and Ham (2004) had focused on such severe violations against the IILS assumption, and improved theory for calculating sap flow with PILS theory, inspired by the work of Ren et al. (2000). The improved theory can avoid underestimates in calculated κ and V_h, up to 10 and 20%, respectively, in the case of a typical probe configuration (i.e., 8-s heating duration and 0.6-cm needle spacing) by Schaeffer et al. (2000). For methods, for instance HR method, the requisite κ and sapwood water content (θ) are mostly determined from destructive wood core measurement. Wood cores are

* Corresponding author at: No. 26 Xinong Road, Yangling 712100, Shaanxi, China.
E-mail address: fanjun@ms.iswc.ac.cn (J. Fan).

https://doi.org/10.1016/j.agrformet.2018.09.009
Received 12 March 2018; Received in revised form 10 August 2018; Accepted 12 September 2018

usually taken from tree only once and the estimated κ and θ are taken as constants in J estimation during the entire sap flow observation period. There would be a loss of accuracy from neglecting temporal variations in κ and θ, probably resulted from plant water-status and seasonal changes. Moreover, deriving κ from wood core measurement, linked to the measured wood density and θ, often misinterprets the correct κ context and neglects the anisotropic nature of sapwood properties (Vandegehuchte and Steppe, 2012a, b; Vandegehuchte and Steppe, 2012d).

Wood is clearly an anisotropic material with vascular structure, an adaption to axial water and nutrient transport in xylem (Backman and Lindberg, 2001). As early as six decades ago, Marshall (1958) had stated that wood is not isotropic, there is a distinct difference between thermal conductivity in axial direction (λ_{ax}) and in tangential direction (λ_{tg}). As stated by Vandegehuchte and Steppe (2012d), λ_{tg} are smaller, on average, 54 ± 7.5% of λ_{ax} cross all dry wood densities and water contents, by applying the equations as mentioned in Swanson (1983). As in literatures where HR methods are applied, the equations of Swanson (1983) have also been widely used to derive thermal diffusivity ($\kappa = \lambda/C$), however, only in axial direction is taken into account. Similarly, Tmax method can estimate κ as aforesaid directly in axial direction, and it is also adopted in the external heat ratio method (Clearwater et al., 2009) for thin stems, pedicels and petioles. Nevertheless, these HP techniques are still based on the key equations of heat conduction-convection in isotropic media.

Only recently were concerns with respect to the application of the isotropic equation for heat transport in anisotropic media raised (Vandegehuchte and Steppe, 2012c, d). Vandegehuchte and Steppe (2012d) proposed an analytical solution of heat conduction-convection equation with IILS considering anisotropy. They numerically simulated the heat transport in the anisotropic sapwood, and confirmed the temperature field around the heater are clearly different due to the difference in axial- and tangential thermal diffusivity (i.e., κ_{ax} and κ_{tg}, respectively), with the isotropic κ taken as the geometric mean of κ_{ax} and κ_{tg}. Such difference in temperature field leads to a difference in t_m for the Tmax method, and clearly influences the ratio of temperature changes for the HR method. Vandegehuchte and Steppe (2012d) further stated that, if the anisotropic κ_{ax} is coupled to temperatures simulated by the isotropic equation, or if the otherwise κ is considered isotropic and the anisotropic equation is applied, erroneous results will emerge in determining J for both Tmax and HR methods. Vandegehuchte and Steppe (2012d) deduced that, existing HP methods based on the inaccurate, isotropic equation – for instance, Tmax and HR methods – remain valid as if the correct anisotropic theory is applied. However, for numerical simulations or the use of inverse optimization techniques, etc., where anisotropic effect can't be canceled out, a solid basis of anisotropic equation must be required.

Vandegehuchte and Steppe (2012c) updated the analytical solution of heat transport equation considering both the finite heating duration and anisotropy, by combining the work of Kluitenberg and Ham (2004) and Vandegehuchte and Steppe (2012d). This theoretical updates directly led to the development of a novel "sapflow+" technique using a four-needle heat pulse sensor, enabling non-empirical J and θ determinations. Yang and Jones (2009) and Yang et al. (2013) developed an inverse method for simultaneous determination of porous media κ, λ and V_h using a penta-needle heat-pulse probe (PHPP) with an INV-WATFLX code based on two-dimensional heat conduction-convection equation in isotropic media by Ren et al. (2000). Sheng et al. (2016) provided a technical instruction to this PHPP and coupled it with an electromagnetic sensor for porous media multi-functional sensing. This smart probe communicates with an SDI-12 interface and performs onboard parameter optimization (Sheng et al., 2016), which is more user-friendly and suitable for general scientific use without expertise in HP measurement techniques. The extension of these smart sensors to include sensing in anisotropic porous media, for instance sapwood, should be of great interest, once the anisotropic effect is carefully considered.

The objectives of this study were to numerically and physically evaluate the impact of anisotropy and PHPP installation angle when determining sapwood sap-flux density and thermal properties. Numerical simulations of heat-pulse measurements using prescribed thermal properties and heat velocities under anisotropic conditions were employed. Numerically derived data were set as input conditions in INV-WATFLX code to retrieve the estimated parameters to match PHPP performance in an anisotropic medium. Field tests were also conducted using six PHPPs on poplar trees with α = 0°, 15° and 30° installation angles.

2. Materials and methods

2.1. Theoretical considerations

Two-dimensional heat conduction-convection (assuming conductive heat dominates over convective effects) for uniform transport of water in an incompressible isotropic porous medium can be expressed as

$$\frac{\partial T}{\partial t} = \kappa\left(\frac{\partial^2 T}{\partial x^2} + \frac{\partial^2 T}{\partial y^2}\right) - V_x\frac{\partial T}{\partial x} - V_y\frac{\partial T}{\partial y} \quad (1)$$

where T is temperature (°C), t is time (s), κ is thermal diffusivity ($m^2\,s^{-1}$), x and y are spatial coordinates in a plane normal to the needles (m) as shown in Fig. 1, V_x and V_y are components of heat velocity V_h ($m\,s^{-1}$), in the respective coordinates. An analytical solution to a PILS injected into an infinite and isotropic medium is given by Ren et al. (2000) and Yang et al. (2013):

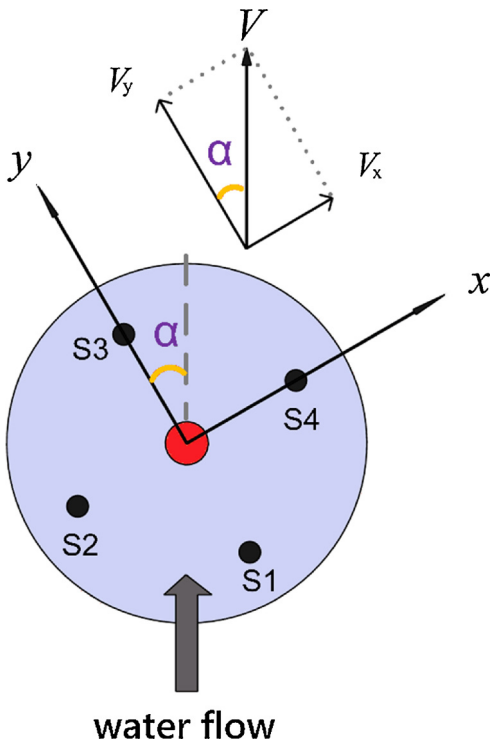

Fig. 1. Schematic illustration of the locations of the heater needle (red) and four thermistor needles (S1–S4) of the penta-needle heat-pulse probe (PHPP) in a coordinate system within a plane normal to the probe axis. Symbols V_x and V_y are the two components of the heat velocity (V_h, $m\,s^{-1}$). (For interpretation of the references to colour in this figure legend, the reader is referred to the web version of this article.)

$$T(x, y, t) = \begin{cases} \frac{q'}{4\pi C\kappa} \int_0^t s^{-1} \exp\left[-\frac{(x - V_x s)^2 + (y - V_y s)^2}{4\kappa s}\right] ds, & 0 < t < t_0 \\ \frac{q'}{4\pi C\kappa} \int_{t-t_0}^t s^{-1} \exp\left[-\frac{(x - V_x s)^2 + (y - V_y s)^2}{4\kappa s}\right] ds, & t > t_0 \end{cases} \quad (2)$$

where q' is the heat input per unit length per unit time (J m^{-1} s^{-1}), C is heat capacity (J m^{-3} °C^{-1}) and t_0 is the heat pulse duration (s). Hereafter we refer to Eq. (2) as the isotropic equation. The temperature at each thermistor needle can be expressed by substituting the coordinates of its location into Eq. (2). The advantage of employing four thermistor needles is the ability to qualify both magnitude and direction of substrate water-flux density and thermal properties in four directions between the heater and each thermistor needle within the sensor's two-dimensional plane illustrated in Fig. 1.

The magnitude and direction of V_h can be obtained from its components, V_x and V_y, as

$$V_h = \sqrt{V_x^2 + V_y^2} \quad (3)$$

or as

$$V_h = V_x \sin\alpha + V_y \cos\alpha \quad (4)$$

where the angle α denotes a clockwise rotation from the y-axis reference (°) as shown in Fig. 1, written

$$\alpha = \tan^{-1}\left(\frac{V_x}{V_y}\right) \quad (5)$$

The magnitude of water-flux density (J, m s^{-1}) is obtained from V_h as

$$J = V_h \frac{C}{C_w} \quad (6)$$

where C_w is the heat capacity of water (J m^{-3} °C^{-1}). The water content of a porous medium (θ, cm^3 cm^{-3}) can be derived from (Yang et al., 2013)

$$\theta = \frac{1}{c_w}\left(C - \rho_b c_b\right) \quad (7)$$

where c_w is the specific heat capacity of water (J kg °C^{-1}), and ρ_b and c_b are bulk density (kg m^{-3}) and specific heat capacity (J kg °C^{-1}) of the dry porous medium, respectively.

When it comes to the heat transport in anisotropic media, such as sapwood, the correct two-dimensional heat conduction-convection relationship for uniform water transport in the axial direction of an anisotropic porous medium, can be expressed as:

$$\frac{\partial T}{\partial t} = \kappa_{tg}\frac{\partial^2 T}{\partial x^2} + \kappa_{ax}\frac{\partial^2 T}{\partial y^2} - V\frac{\partial T}{\partial y} \quad (8)$$

where κ_{ax} and κ_{tg} are axial- and tangential thermal diffusivity, respectively. Correspondingly, the correct analytical solution for PILS in an infinite and anisotropic medium becomes (Vandegehuchte and Steppe, 2012c):

$$T(x, y, t) = \begin{cases} \frac{q'}{4\pi C\sqrt{\kappa_{ax}\kappa_{tg}}} \int_0^t s^{-1} \exp\left[-\left(\frac{(x - V_x s)^2}{4\kappa_{tg} s} + \frac{(y - V_y s)^2}{4\kappa_{ax} s}\right)\right] ds, & 0 < t < t_0 \\ \frac{q'}{4\pi C\sqrt{\kappa_{ax}\kappa_{tg}}} \int_{t-t_0}^t s^{-1} \exp\left[-\left(\frac{(x - V_x s)^2}{4\kappa_{tg} s} + \frac{(y - V_y s)^2}{4\kappa_{ax} s}\right)\right] ds, & t_0 < t \end{cases} \quad (9)$$

We now refer to Eq. (9) as the anisotropic equation.

2.2. Penta-needle heat pulse probe (PHPP)

The PHPP is comprised of a main circuit board with all the electronic elements soldered to the head circuit board housing five stainless needles. The central heater needle (o.d. 2.1 mm, outer length 28 mm) is surrounded by four thermistor needles (o.d. 1.27 mm, outer length 16 mm) orthogonally arranged with an equal radial distance 6.5 mm to the heater needle. In practice, it doesn't generate an ideal infinite line source due to finite needle length (L) and diameter (d). However, Blackwell, 1956 stated that the axial-flow error is less than 1%, if it satisfies $L/d > 25$. Later, Kluitenberg et al. (1995) indicated that errors of estimated κ and C are less than 2%, if it satisfies $L/d > 4.4$ and $d/r < 0.26$. The PHPP operating under the INV-WATFLX code is based on isotropic theory for simultaneous inverse estimation of V_x, V_y, κ and λ within a plane normal to the needles. Subsequently C is calculated and θ is determined, across a range of J up to 300 cm h^{-1}. The code is insensitive to the influence of α in isotropic porous media (Sheng et al., 2016; Yang and Jones, 2009; Yang et al., 2013). The on-board microcontroller controls the inverse optimization of parameters κ, λ, V_x and V_y by fitting a sequence of measured temperature rise data following a heat pulse injection. The default heat-pulse duration is 8 s and temperature is recorded over 120 s at each of the four thermistor needles. The optimization fits Eq. (2) to temperature rise data by adjusting the thermal properties and heat velocities, employing the robust Gauss-Newton–Levenberg–Marquardt method (see Yang and Jones, 2009; Yang et al., 2013; Sheng et al., 2016).

2.3. Numerical simulation of INV-WATFLX application in anisotropic media

Numerical simulation software (Mathematica 11.0, Wolfram Research http://www.wolfram.com) was applied to model PHPP heat-pulse measurement using the isotropic equation in anisotropic media as illustrated in the flowchart of Fig. 2. Prescribed initial thermal properties were taken from a softwood (dry wood density = 350 kg m^{-3}; water content = 1.3 kg kg^{-1}, in water weight per unit dry wood weight) calculated from Burgess et al. (2001), and V_h varied between 0 and 210 cm h^{-1} in increments of 30 cm h^{-1}. The corresponding range of J calculated from Eq. (6) is from 0 to 130 cm h^{-1}, which is within the natural sap-flux density range (0–110 cm h^{-1}), according to Vandegehuchte and Steppe (2012c) and Vertessy et al. (1997). Simulations also included prescribed installation angles, α, from 0° to 90° at intervals of 5°. Anisotropy degree, κ_{tg}/κ_{ax}, varied between 0.5 to 1 at intervals of 0.05 (Table 1), where for a given κ_{tg}/κ_{ax} value, κ_{tg} and κ_{ax} were resolved from the overall κ. Prescribed α (Fig. 1) dictated positions of the four thermistors (S1–S4) and facilitated decomposition of V_h into its two components V_x (= V_h sin α) and V_y (= V_h cos α). The coordinate system was defined with the y-axis positive upward (axial direction) and the x-axis positive to the right (tangential direction). Simulation of the PHPP heat pulse required further prescription of sensor-related parameters, such as i) heater-thermistor spacing, r, ii) heating strength, q', and iii) heat pulse duration, t_0, (i.e., based on heat pulse sensor technical specifications). Eq. (9) was subsequently used to simulate heat pulse-based temperature rise data at 1 s intervals for 120 s at each of the 4 thermistor positions, S1 - S4. Subsequently the coordinate system transitions from the numerical model to the probe needle-face coordinate system shown in Fig. 1, which is next employed by the INV-WATFX algorithm. The temperature rise data are subsequently used as input to the INV-WATFLX code, which was reprogrammed in Mathematica language following the algorithm instruction provided by Yang and Jones (2009) and Yang et al. (2013), to inversely optimize κ, λ, V_x and V_y and imitate the PHPP function. This allowed comparison of the optimized κ, λ, V_x and V_y values in the PHPP code and their prescribed values in order to evaluate the impact of anisotropy and α. We expected to develop a correction model following the numerical simulation, and to apply to sap-flux density and thermal properties estimation for anisotropic media.

2.4. Field experiments

Field tests were performed on a poplar (*Populus simonii* Carr.) tree in

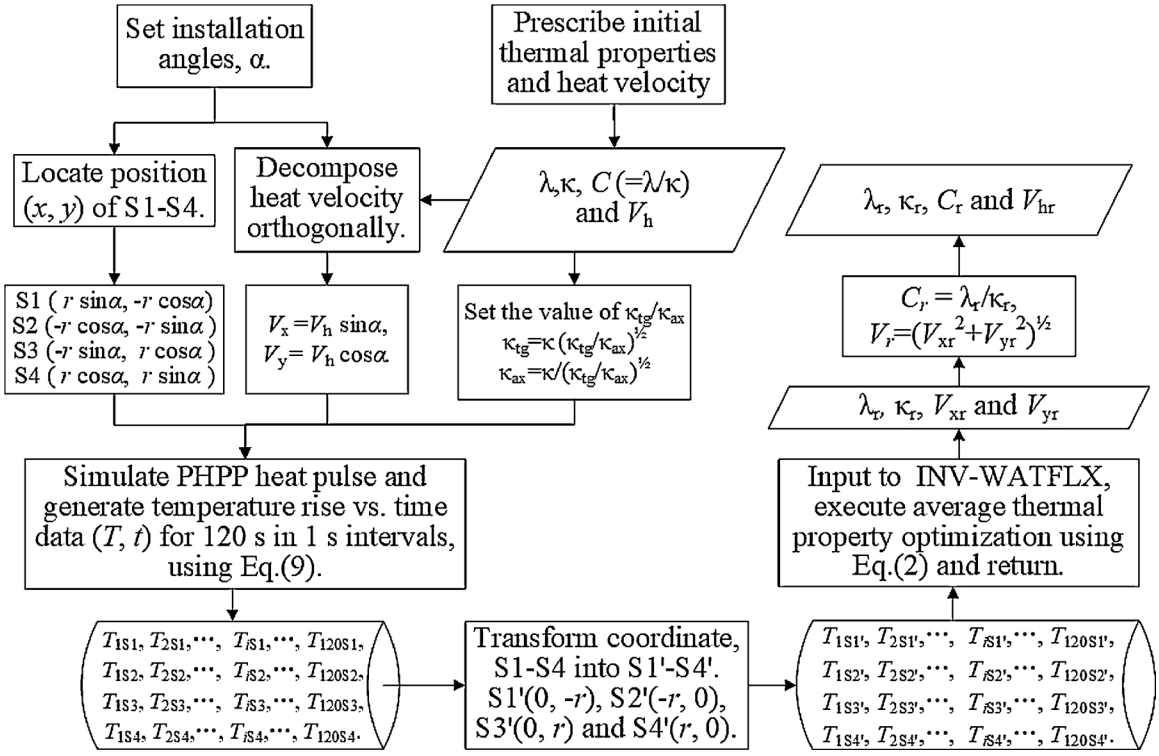

Fig. 2. Flowchart of the numerical simulation process for applying INV-WATFLX algorithm in anisotropic media. Subscript *i* is time lag and S1–S4 represent thermistor coordinate positions shown within the cylinders. Additionally, S1'–S4' represent their positions within the probe's needle-face coordinate system (see Fig. 1). Subscript *r* indicates parameters optimized using the INV-WATFLX algorithm.

Table 1
Conditions used to simulate heat transport in the anisotropic sapwood, where κ_{tg} and κ_{ax} represent tangential- and axial thermal diffusivity, respectively, and the axial direction of heat velocity is upward. When $\kappa_{tg}/\kappa_{ax} = 1$ isotropic conditions applies; for $\kappa_{tg}/\kappa_{ax} < 1$, the degree of anisotropy increases as the ratio decreases.

Parameters, units	Symbol	Value	Intervals
Installation angle, °	α	0–90	5
Degree of anisotropy	κ_{tg}/κ_{ax}	1.0–0.5	0.05
Overall thermal conductivity, $W\,m^{-2}\,°C^{-1}$	λ	0.5	
Overall thermal diffusivity, $10^{-6}\,m^2\,s^{-1}$	κ	0.2	
Magnitude of heat velocity, $cm\,h^{-1}$	V_h	0 to 210	30

the Liudaogou catchment (1200 m altitude, 38.78°N, 110.35°E) of Shenmu County, Shaanxi Province, China. The catchment is within the Loess Plateau referred to as the "water-wind erosion crisscross region". The selected poplar tree was planted in a check-dam system about 40 years ago and was healthy and exhibiting robust growth and development, with average tree height 27.8 m and diameter at breast height 50.9 cm. The surrounding soil conditions provided ample root water from both natural rainfall and abundant shallow groundwater. The main soil type was a loess soil, consisting of 52.5% sand (> 0.05 mm), 35.8% silt (0.002–0.05 mm) and 11.7% clay (< 0.002 mm).

Before PHPPs were applied in field sap flow experiment, the effective distance between the heater- and each temperature needle (i.e., needle spacing) was carefully calibrated within a static saturated sand (0.1–0.25 mm particle diameter) column. Specific heat capacity of the dry sand sample was measured by differential scanning calorimetry using a STA 449 F3 Jupiter® simultaneous thermal analyzer (Netzsch Group, Selb, Germany). Water content of the saturated sand were measured, and then *C* was derived according to Eq. (7) in Sheng et al. (2016). Six PHPPs were installed in the sand column, and spacing calibration was triggered by calibration command with assigned user-defined *C* through CR1000 measurement system (Campbell Scientific, Logan, UT). See spacing calibration details in Sheng et al. (2016).

The six PHPPs were then removed from sand column and installed within the same aspect of the tree trunk at breast height. Before installation, the coarse bark was removed, and an electric drill and jig were used to bore five vertically aligned holes to tightly match the PHPP's needle geometry. Three installation angles of α = 0°, 15° and 30° were employed, with duplicates of each angle. Probes were axially arranged with a spacing of 10 cm, with no overlapping probes in the vertical sap flow pathway. They were connected to a CR850 data logger (Campbell Scientific, Logan, UT), and λ, κ, V_x and V_y were fitted and recorded at hourly intervals. Values of *C* obtained through the relationship $C = \lambda/\kappa$, and V_h and *J* were calculated from Eqs. (4) and (6), respectively. Deviations of these estimated parameters from anisotropy effects would be removed through a correction model expected to be developed in this study.

Three TDPs were inserted in sapwood 20 cm above the uppermost PHPPs to provide additional *J* estimates for comparison. TDP method is one of most commonly used empirical sap flow approaches owing to its simplicity, the high degree of accuracy and reliability, and its relatively low-cost (Lu et al., 2004). Early calibration experiments of TDPs on two common types of stem species, i.e., diffuse-porous trees and ring-porous trees, reported generally good agreement with the original calibration of Granier (1987) for diffuse-porous species (Bush et al., 2010), describing the poplar trees used here. Details concerning TDP construction and methodology are given in our previous study by Peng et al. (2015). They were connected to a CR1000 data logger, and *J* was collected at hourly intervals.

3. Results

3.1. Heat field discrepancy in anisotropic media

An anisotropic medium such as sapwood exhibits a higher axial

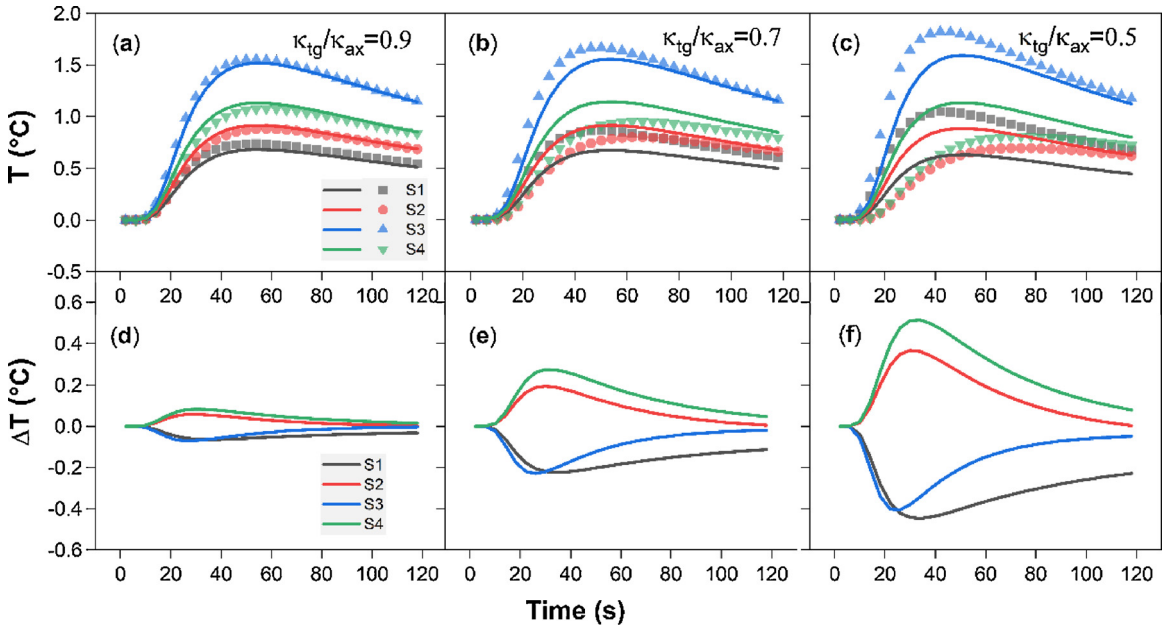

Fig. 3. Examples of fitted temperature rise using the isotropic Eq. (2) for simulated T versus time (s) data in anisotropic media. Prescribed parameters are: $\alpha = 15^{\circ}$, $\kappa = 2 \times 10^{-7}$ $m^2 s^{-1}$, $\lambda = 0.5$ $W m^{-1} s^{-1}$, $C = 2.5 \times 10^{-7}$ $J m^{-3} °C^{-1}$, $V_h = 90$ $cm h^{-1}$ and $\kappa_{tg}/\kappa_{ax} = 0.9$ (a), 0.7 (b) and 0.5 (c). Four symbols denote simulated temperature rise versus time data in anisotropic media in a heat pulse measurement at four thermistor positions (S1–S4). In (a)–(c), lines with four different colors represent fitted temperature rises (T, °C) at four thermistor positions (S1–S4); in (d)–(f), lines describe the corresponding temperature discrepancies (ΔT, °C) between the fitting curves using isotropic Eq. (2) and simulated temperature rise using anisotropic Eq. (9) at four thermistor positions.

thermal diffusivity than its tangential thermal diffusivity, causing a disparity in heat conduction axially versus tangentially within a given trunk ring (e.g., from a line heat source inserted horizontally into the trunk). As the difference of thermal diffusivity in two directions grows (i.e., a smaller κ_{tg}/κ_{ax}), relatively less heat is transported tangentially, resulting in a narrower and axially longer heat field. Fig. 3(a–c) shows examples of heat transport signatures measured at the four thermistors (S1–S4) of a PHPP for $\alpha = 15^{\circ}$ using three different κ_{tg}/κ_{ax} scenarios. Temperature difference between S1 and S3, which are closer to the axial flow direction, are larger than temperature difference between S2 and S4, which are closer to the tangential direction. Discrepancies of fitted temperature rise for each needle, show a substantial increase as κ_{tg}/κ_{ax} becomes smaller (greater anisotropy). The maximum discrepancies at S3 and S1 were 0.47 and 0.37 °C, and at S2 and S4 were −0.29 and −0.38 °C for $\kappa_{tg}/\kappa_{ax} = 0.5$. Fig. 3(d–f) describe the differences between the isotropic and anisotropic temperature rise for $\kappa_{tg}/\kappa_{ax} = 0.9$, 07 and 0.5. The difference climbs to approximately 0.5 °C for $\kappa_{tg}/\kappa_{ax} = 0.5$, while it is less than 0.1 °C and shows good agreement for $\kappa_{tg}/\kappa_{ax} = 0.9$. Thus, large errors may arise even without considering the anisotropic conditions found in sapwood.

3.2. Deviation analyses of the applied INV-WATFLX algorithm in anisotropic media

Heat velocities, V_h, inversely estimated from application of the INV-WATFLX code, exhibit significant linear correlation with the prescribed V_h, that varied between 0–210 $cm h^{-1}$ ($R^2 > 0.99$ and $P < 0.01$), as κ_{tg}/κ_{ax} varied from 1.0 to 0.5 and α varied between 0° and 90°. Fig. 3 shows a comparison of V_h estimated and prescribed under different κ_{tg}/κ_{ax} and α scenarios. Fig. 4 further illustrates a slope change as V_h is compared for α increasing from 0° to 45°. There we see the gradual transition from a slope above 1.0 to a slope less than 1.0, indicating an overestimate that transitions to an underestimate in V_h. Digging deeper, for $\kappa_{tg}/\kappa_{ax} = 0.8$, the slope range is from 1.099 to 0.907, while for $\kappa_{tg}/\kappa_{ax} = 0.5$, the range extends to between 1.396 and 0.708 considering the selected α values shown in Fig. 4. The greater the anisotropy (lower value of κ_{tg}/κ_{ax}), the higher the deviation in the V_h estimate.

Estimated κ, λ and thus C are also affected by anisotropy. Fig. 5 illustrates the intensity of deviations (%) of estimated thermal properties as influenced by both α and V_h at $\kappa_{tg}/\kappa_{ax} = 0.5$. The deviation is the difference in fitted properties applying the INV-WATFLX algorithm in anisotropic media. Summarizing these effects, α contributes to a sharper deviation than V_h on estimated κ, λ and C, and the deviation is symmetric around $\alpha = 45^{\circ}$. Deviations in C transit from a slight underestimate at 0° and 90° to a higher overestimate at 45° and using higher values of V_h, while λ exhibits the opposite trend with underestimates at 45° and overestimates at the extents. On the other hand, κ only shows overestimates, which increase with V_h and extending from 45° each way.

Fig. 6 gives a more comprehensive perspective of the impact of anisotropy on estimated V_h, J, C, κ and λ. For $\kappa_{tg}/\kappa_{ax} = 1$, i.e., in isotropic media, no deviations occur when applying the INV-WATFLX code regardless of the value of α. However, as κ_{tg}/κ_{ax} gets smaller, parameter deviations subsequently emerge and enlarge, and show stronger influence from α. Deviations in V_h (Fig. 6a) and J (Fig. 6b) are similar up to nearly 40% and as low as -30% for $\kappa_{tg}/\kappa_{ax} = 0.5$. Deviations in C, κ and λ are far smaller, in most cases < 10%, under static conditions as shown in Fig. 6(c–e). Given the growing interest for application of PHPP in porous media such as sapwood, which exhibit different degrees of anisotropy coupled with diverse possible installation angles, there is a need for a correction algorithm that can provide reliable probe calibration in terms of known κ_{tg}/κ_{ax} and α values. We therefore developed a function according to simulation results to describe the relationship between these relative deviations (ε, %) and κ_{tg}/κ_{ax} and α, written:

$$\varepsilon = 100 \cdot a \left[\frac{1 - \kappa_{tg}/\kappa_{ax}}{1 + \kappa_{tg}/\kappa_{ax}} \right]^{b} (\cos 4\alpha + c) \quad (10)$$

where ε denotes the relative deviation (%) of estimated V_h (including components within the coordinate systems), J, C, κ and λ. Coefficient b is assigned according to specific evaluated properties, and a, c are coefficients from non-linear regression fitting of Eq. (10) using the simulation results. These coefficients are listed in Table 2.

If we use p_r to symbolize the specific raw parameters listed in

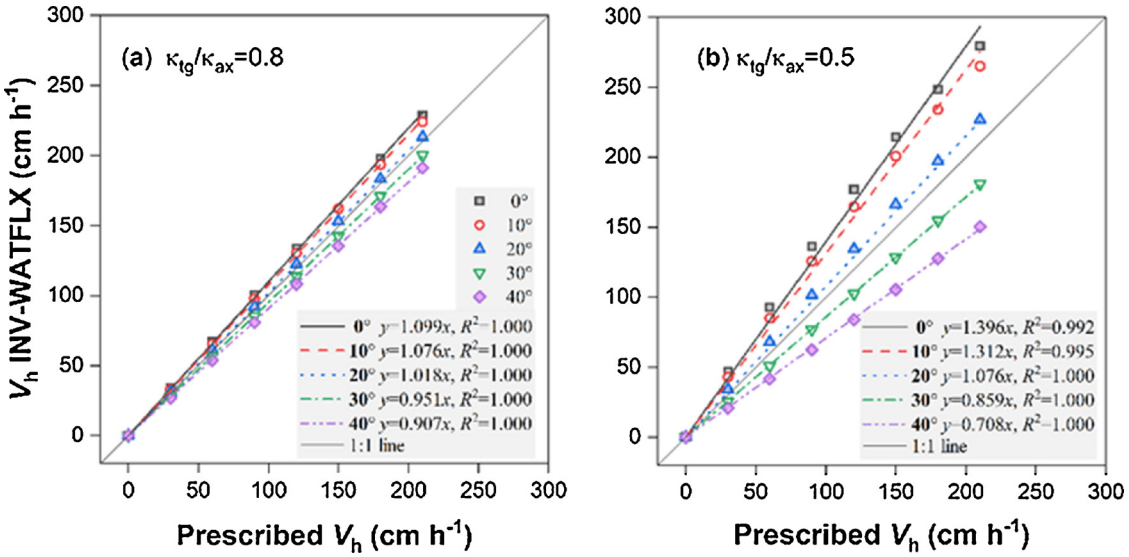

Fig. 4. Examples of heat velocity (V_h, cm h^{-1}) inversely estimated by applying the INV-WATFLX code using installation angles, α, of between 0°–40° in 10° intervals versus the prescribed V_h values in anisotropic media using κ_{tg}/κ_{ax} = 0.8 (a) and = 0.5 (b), respectively. Regression functions (lines) and R^2 values are also listed.

Table 2 before anisotropy effect correction and p_c to symbolize the corresponding corrected parameters, then p_c is given as

$$p\ c = A \cdot pr \tag{11}$$

where A denotes the relevant correction multiplier. The relationship between A and ε is expressed as

$$A = \frac{1}{1+0.01\cdot\varepsilon} \tag{12}$$

As to sapwood, the value of κ_{tg}/κ_{ax} is approximately equal to 0.5. A set of values of ε and A under different installation angles can be calculated and to apply to anisotropy effect correction in sap-flux density and thermal properties determination.

3.3. Field tests

Field tests were conducted from June 5 to July 24, 2017, lasting 50 days. The value of κ_{tg}/κ_{ax} obtained in the poplar (*Populus simonii* C.) sapwood was 0.524 ± 0.007, determined from PHPP measurements using individual thermal property parameter optimization at 0° installation angle (not discussed in this paper, see Sheng et al., 2016). It agreed well with the range of sapwood κ_{tg}/κ_{ax} given by Vandegehuchte and Steppe (2012d). Table 3 shows values of the correction multiplier, A, used to adjust PHPP-based parameter estimates obtained in the poplar sapwood for each of the three installation angles. Raw parameter estimates from the PHPPs were corrected with Eq. (11) and the multipliers shown in Table 3. Fig. 7 shows the corrected hourly V_x and V_y dynamics. For $\alpha = 0°$, V_x ranged from −0.78 to 3.05 cm h^{-1} and averaged 0.74 cm h^{-1}, V_y values ranged from −1.54 to 39.73 cm h^{-1} and averaged 12.64 cm h^{-1}, confirming that the heat velocity distribution was mainly oriented along the y-axis as expected. For $\alpha = 15°$, V_x ranged from −0.89 to 18.48 cm h^{-1} and averaged 6.36 cm h^{-1}, V_y ranged from −1.31 to 61.12 cm h^{-1} and averaged 16.80 cm h^{-1}. For $\alpha = 30°$, V_x ranged from −1.07 to 30.44 cm h^{-1} and averaged 8.45 cm h^{-1}, V_y extended from −2.74 to 46.34 cm h^{-1} and averaged 14.72 cm h^{-1}. The difference between the x- and y-axis heat velocity values decreased as α increased.

Dynamics of corrected κ, λ and C are illustrated in Fig. 8(a–c), where all show diurnal fluctuations to different extents. Comprehensively, estimated values of κ, λ and C at $\alpha = 0°$ were steadier and revealed lower fluctuations than at 15° and 30°. For $\alpha = 0°$, the daily maximum fluctuations in κ, λ and C were 1.7%, 22.4% and 28.7%, respectively. Fluctuations for $\alpha = 15°$ were 32.7%, 56.0% and 17.2% and for $\alpha = 30°$ they were 26.6%, 56.6% and 22.9%, respectively. Hourly thermal properties before dawn 3:00–5:00 a.m., (i.e., during assumed zero-flow conditions), were relatively stable for days at a time

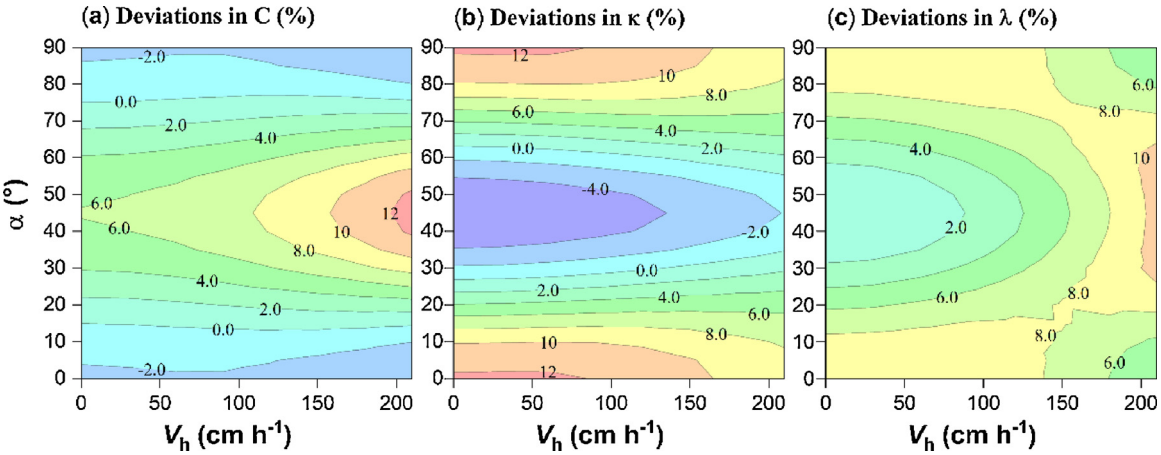

Fig. 5. Contour plots of the deviation (%) of estimated heat capacity, C (a), thermal diffusivity, κ (b), and thermal conductivity, λ (c), by applying the INV-WATFLX code as affected by both heat velocity, V_h (cm h^{-1}), and installation angle, α (°), at κ_{tg}/κ_{ax} = 0.5.

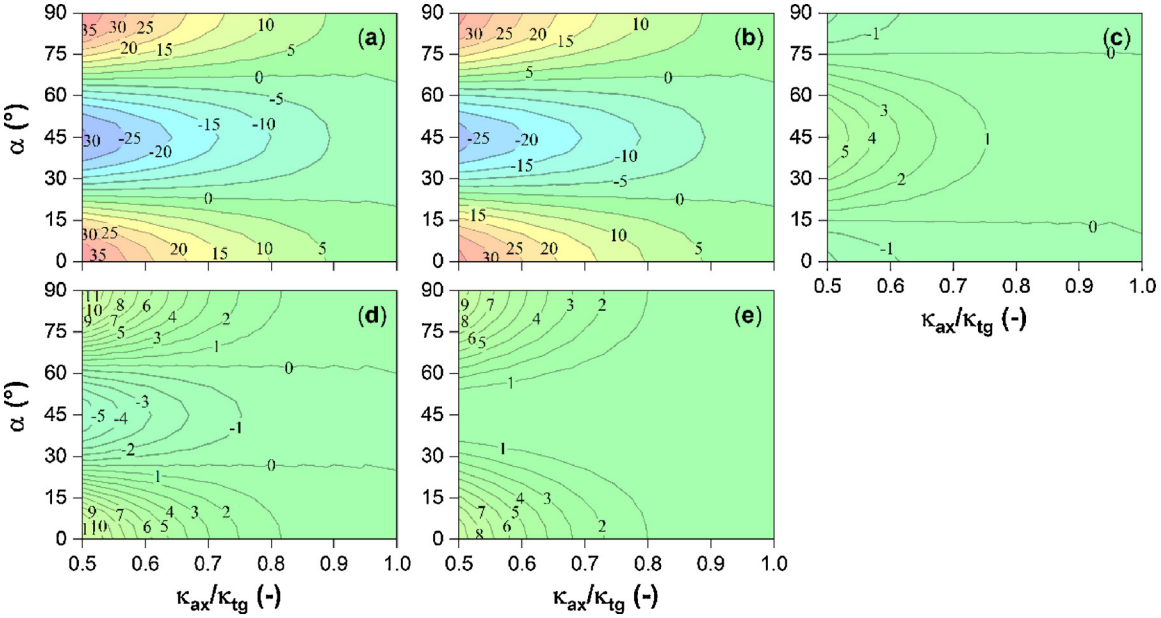

Fig. 6. Contour plots of the deviation (%) of heat velocity, V_h (a), water-flux density J (b) under non-static conditions and the deviation (%) of heat capacity, C (c), thermal diffusivity, κ (d) and thermal conductivity, λ (e) under static conditions estimated by applying the INV-WATFLX code as affected by the degree of anisotropy, κ_{tg}/κ_{ax}, and installation angle, α (°).

Table 2
Coefficients of deviation function. i.e., Eq. (10), obtained from estimated parameters; heat velocity (V_h), water-flux density (J), heat capacity (C), thermal diffusivity (κ) and thermal conductivity (λ).

Parameters estimated	Coefficients			Statistics	
	a	*b*	*c*	*RMSE*	R^2
V_h, V_x and V_y	1.417	1.25	0.078	0.006	0.997
J	1.297	1.25	0.122	0.008	0.995
C	−0.362	2.00	−0.499	0.001	0.999
κ	0.789	2.00	0.322	0.001	0.998
λ	0.429	2.00	0.990	0.001	0.999

Table 3
Correction multipliers, A, in Eq. (12), used to adjust PHPP parameter estimates obtained in poplar (*Populus simonii* C.) sapwood. Corrected parameters included heat velocity (V_h), water-flux density (J), heat capacity (C), thermal diffusivity (κ) and thermal conductivity (λ). The estimated sapwood anisotropy was κ_{tg}/κ_{ax} = 0.524 and three installation angles, α = 0°, 15° and 30° were used.

Parameters estimated	Installation angle, α		
	0°	15°	30°
V_h, V_x and V_y	0.737	0.839	1.162
J	0.746	0.841	1.129
C	1.018	1.000	0.966
κ	0.908	0.940	1.014
λ	0.923	0.941	0.980

over the measurement period. Only slight undulations emerged from nocturnal sap flow in late June and early July as seen in Fig. 7. Such nocturnal sap flow occurred in period as daytime sap-flux density climbed high and as nighttime vapor pressure deficit (VPD) was very high from our observations (data were not shown). Trees might absorb water from soil in nighttime to recover from water deficit in stems due to strong transpiration in daytime, or nocturnal transpiration may occur under high VPD conditions. Green sapwood was sampled on June 13 and July 16, where the bulk density of the dry sapwood, ρ_b, was 0.349 ± 0.013 kg m^{-3}. The sampled sapwood water contents for these dates were 0.468 ± 0.027 and 0.549 ± 0.032 cm^3 cm^{-3}, respectively. Errors of 3.4% and 6.5%, respectively, were found when comparing the two sample dates with water contents derived from Eq. (7) using the obtained heat capacity.

Sap-flux density, J, derived from three installation angles (α = 0°, 15° and 30°) showed accordant trends and strong diurnal variation. Most nighttime sap-flux density readings were close to zero with a few readings in late June and early July of up to 5 cm h^{-1}. The maximum J values were 27.2, 39.1 and 37.2 cm h^{-1} for α = 0°, 15° and 30°, respectively. The corresponding average J values were 8.6, 12.2 and 11.9 cm h^{-1} (Fig. 9a). There was an extremely higher linear correlation of J for the PHPPs among the different installation angles, and R^2 was as high as 0.98 (Fig. 9b). Fig. 10(a) and (b) show the correlation analyses between J determined from PHPPs before and after model calibrations using Eqs. (10)–(12) and J values estimated using TDPs. The PHPP-based values of J were linearly correlated ($P < 0.01$) with TDPs, but R^2 values were approximately 0.8. The linear regression of corrected J at α = 15° and 30° with the TDP data yielded slopes of nearly 1 (1.01 and 0.984, respectively) while for α = 0°, the slope was 0.69, indicating an apparent underestimate.

4. Discussions

The penta-needle heat pulse probe operating under the INV-WATFLX code has been verified as a robust and user-friendly integrated multi-functional sensor in isotropic porous media sensing (Sheng et al., 2016; Yang and Jones, 2009; Yang et al., 2013). Yang and Jones (2009) reported that this PHPP can work properly and the optimized parameters are unaffected even if one in the four thermistor needles is out of use. They showed that this PHPP coupled with INV-WATFLX code is insensitive to the influence of α in isotropic porous media, such as soils. However, from both our numerical simulation and field tests, the direct use of PHPP in sapwood sensing will inevitably cause non-negligible errors in optimized parameters due to anisotropic nature of sapwood. Under a typical case, as sapwood κ_{tg}/κ_{ax} = 0.5 (Steinhagen, 1977), deviations of raw sap-flux density estimated from PHPPs are within a wide range of from −31% to 40%, while κ, λ and C under static conditions attributes a smaller deviation < 10%, differing across installation angles, α, which vary from 0° to 90° (Fig. 7).

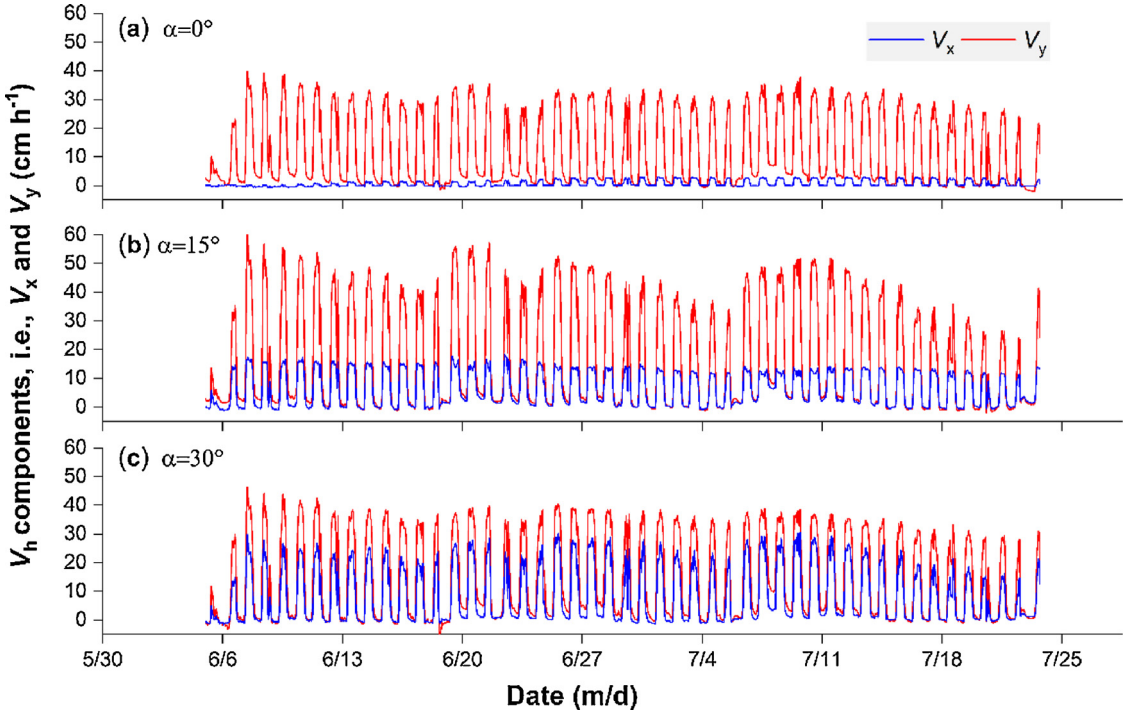

Fig. 7. Corrected heat velocity (V_h) components, V_x and V_y (cm h^{-1}) using Eqs. (10)–(12) and parameters listed in Table 2 with installation angles α = 0° (a), = 15° (b) and = 30° (c).

Selection of the installation angle, α, for multi-needle heat pulse probes has rarely been a focus in soils and other porous media sensing. Theoretically water flux and thermal property estimations is immune to the effects of insertion angle in isotropic media. However, all five parameters are intensely affected by α under heat field deformation owing to anisotropy (Figs. 4–7). The numerical correction models we developed in Eqs. (10)–(12) with coefficients listed in Table 2, provide an effective way to minimize PHPP parameter estimation errors due to anisotropy. This model is ideally suited to the PHPP configuration for anisotropy values in the range of $0.5 \leq \kappa_{tg}/\kappa_{ax} < 1$ and for any value of α. In addition, porous medium anisotropy can be estimated from PHPP measurements leading to individual thermal property parameter optimization (not discussed in this paper, see Sheng et al., 2016) with 0° installation under static conditions. Inaccuracy in α determination possess another potential error source. A 1° error in probe installation angle will generate a theoretical maximum error of 2.5% in J at

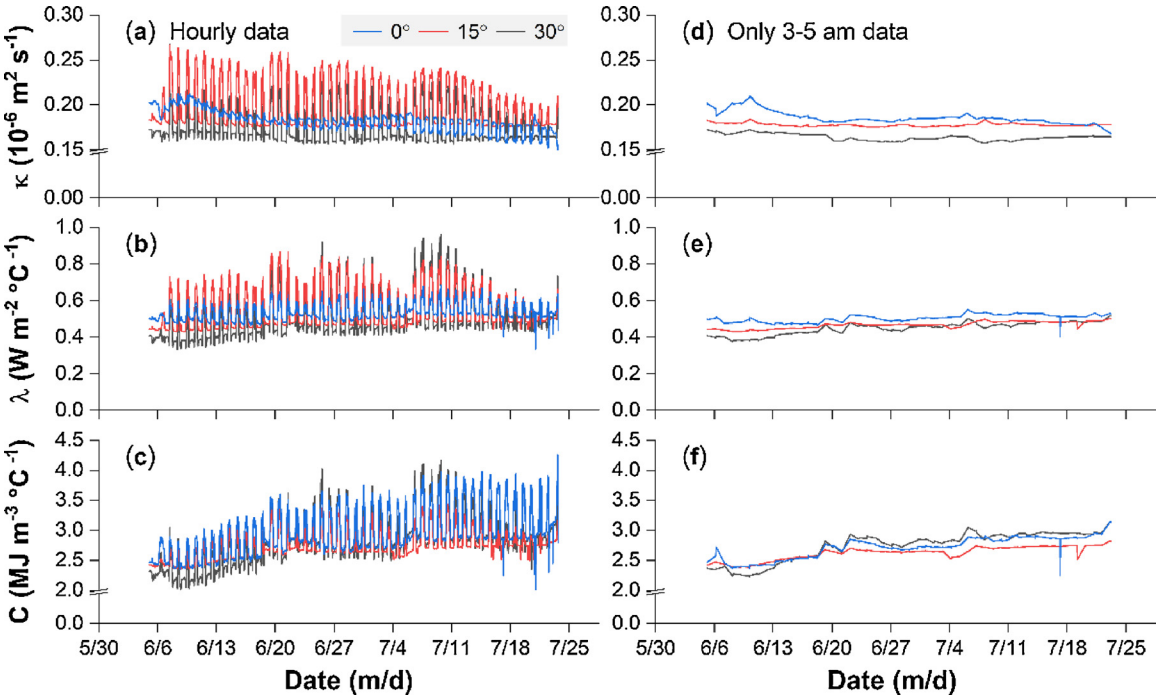

Fig. 8. Corrected thermal properties, C, κ and λ, calibrated with Eqs. (10)–(12), using raw data from PHPPs with installation angle α = 0°, 15° and 30°. Panels (a)–(c) list the continuous hourly data, while panels (d)–(f) report only daily data between 3:00–5:00 am when zero-flow conditions are expected.

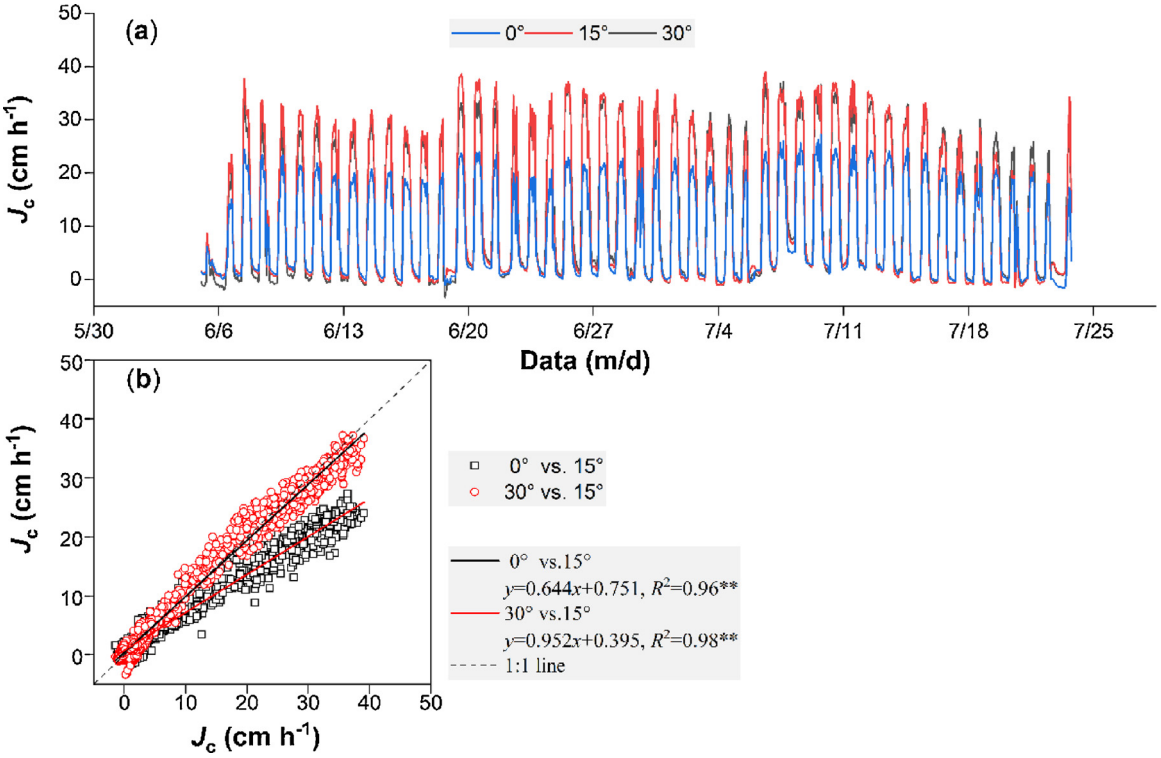

Fig. 9. (a) Corrected sap-flux density (J_c, cm h^{-1}), using Eqs. (10)–(12), estimated with PHPPs at $\alpha = 0°$, 15° and 30°. (b) An correlation analysis of J_c derived from different installation angles, $\alpha = 0°$, 15° and 30°. Symbols ** represent $P < 0.01$.

$\alpha = \sim 22°$ or $\sim 68°$, the sensitivities of κ, λ and C to α errors are much smaller. Those errors also decrease rapidly as α deviates from values of 22° and 68°. From the deviation analysis in Fig. 5, thermal properties are more sensitive than sap-flux density (heat velocity) to variations in installation angle, especially at high velocities for $\alpha < 15°$ or $> 75°$ compared to values within ranges of 15°–30° and 60°–75°. However, we should recognize that, the correction model we developed still remain empirical rather than an analytical model, which could resolve the rationale behind it and greatly promote developments in anisotropic media sensing techniques. Nevertheless, seeking an analytic correction model seems challenging. The analytical solutions of heat transport equation for PILS, i.e., Eqs. (2) and (9), contains the transcendental exponential integral, and numerical solution methods seem the most effective instruments, as "sapflow+" technique and INV-WATFLX algorithm both use. Alternatively, replacing the isotropic equation with anisotropic equation within INV-WATFLX code, and developing an "anisotropic" version of INV-WATFLX algorithm is needed. But it may require updating and improving the probe processing performance, because the "anisotropic" version involves much more parameters in inverse optimization than the "isotropic" version.

Insertion of five needles (PHPP) into a small area of the trunk or stem would damage the sapwood structure and disturb sap flow pathway and cause flow turbulence especially at high sap-flux density (Fig. 8). Flow pathway distortion is a possible cause of fluctuations in inversely optimized κ, λ and C under dynamic sap flow conditions. However, under static conditions, estimated κ, λ and C were observed highly steady for all three tested installation angles. We have a hypothesis that, some sap flow pathways may distort rather than keep vertical around the sensor insertion position, within which heat transport was distinctly more complex than heat transport described in Eq. (9) and resulted in fluctuations in optimized thermal properties at high flow conditions. During field tests, J was underestimated by more than 30% at $\alpha = 0°$ as compared with $\alpha = 15°$ and 30°, and results of TDPs. From the PHPP construction structure, the center heater needle is

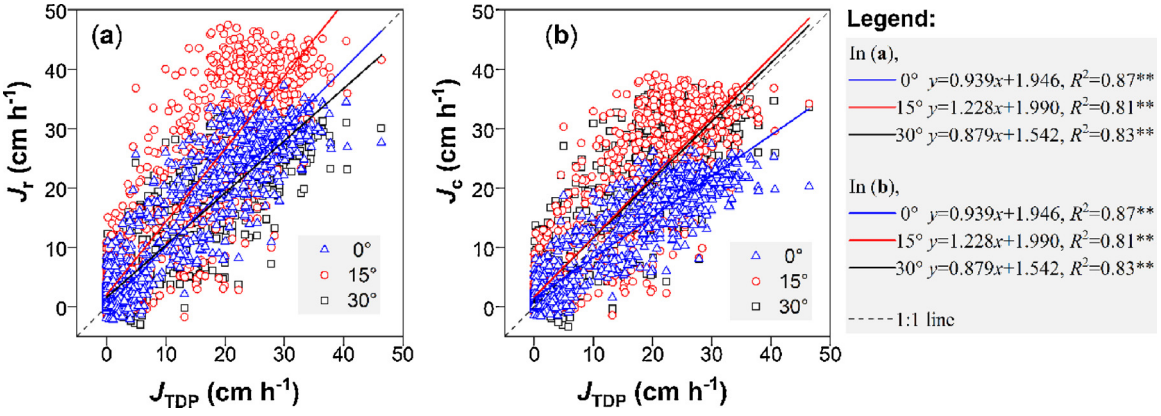

Fig. 10. Correlation analyses between sap-flux densities estimated from TDPs (J_{TDP}, cm h^{-1}) and (a) raw- and (b) corrected sap-flux density using Eqs. (10)–(12) from PHPPs (J_r and J_c, respectively; cm h^{-1}) under different installation angles, $\alpha = 0°$, 15° and 30°. Symbols ** represent $P < 0.01$.

remarkably 65% larger than the adjacent thermistor needles in diameter, and there may generate a small less hydraulically active zone, straight up and down the inserted heater. When PHPP is inserted at $\alpha = 0^{\circ}$, as two thermistor needles sit straight up and down the center heater, large underestimation in J occurs. Heretofore, heat-pulse based sap flow methods, including CHP, Tmax, HR and "sapflow+" method, have employed probes needles aligned vertically. They were widely observed underestimating J, and utilized numerical correlations with respect to wound size, especially for CHP and HR methods (Burgess et al., 2001; Green et al., 2003; Steppe et al., 2010; Swanson and Whitfield, 1981). However, Using the PHPP coupled with the INV-WATFLX algorithm accommodates rotation from vertically aligned needle installation and provides a two-dimensional heat velocity and thermal property inverse fitting routine. Though the calibration model we developed potentially minimizes errors due to application of the isotropy equation in sapwood, the PHPP still faces potential estimation errors derived from flow turbulence, which is more complex to model. Now, systematic studies concerning sap flow disturbance/turbulence caused by inserted needles are still rare. In future, flow distribution map around inserted needles can be traced by techniques such as nuclear magnetic resonance (Nybo et al., 2018) to provide a perceptive approach to investigate their impacts. This study has presented a general introduction of the PHPP measurement and modeling for anisotropic sapwood sensing. Further means of testing such as gravimetric validation experiments and higher resolution measurement approaches should be applied to develop a more systematic and comprehensive awareness of sap/water flux and thermal property estimation in anisotropic media.

Conflicts of interests

The authors declare that there are no conflicts of interest.

Acknowledgements

The authors would give thanks to the support from the Projects of National Natural Science Foundation of China [NSCF 41571130082, 41271239]. We would also thank the editors and the anonymous reviews for their diligent work and pertinent, valuable suggestions.

References

Backman, A.C., Lindberg, K.A.H., 2001. Differences in wood material responses for radial and tangential direction as measured by dynamic mechanical thermal analysis. J. Mater. Sci. 36 (15), 3777–3783. https://doi.org/10.1023/A:1017986119559.

Blackwell, J.H., 1956. The axial-flow error in the thermal-conductivity probe. Can. J. Phys. 34 (4), 412–417. http://www.nrcresearchpress.com/doi/abs/10.1139/p56-048.

Burgess, S.S., Adams, M.A., Turner, N.C., Beverly, C.R., Ong, C.K., Khan, A.A.H., Bleby, T.M., 2001. An improved heat pulse method to measure low and reverse rates of sap flow in woody plants. Tree Physiol. 21 (9), 589–598. https://doi.org/10.1093/treephys/21.9.589.

Bush, S.E., Hultine, K.R., Sperry, J.S., Ehleringer, J.R., 2010. Calibration of thermal dissipation sap flow probes for ring- and diffuse-porous trees. Tree Physiol. 30 (12), 1545–1554. https://doi.org/10.1093/treephys/tpq096.

Clearwater, M.J., Luo, Z.W., Mazzeo, M., Dichio, B., 2009. An external heat pulse method for measurement of sap flow through fruit pedicels, leaf petioles and other small-diameter stems. Plant Cell Environ. 32 (12), 1652–1663. https://doi.org/10.1111/j.1365-3040.2009.02026.x.

Cohen, Y., Fuchs, M., Green, G.C., 1981. Improvement of the heat pulse method for determining sap flow in trees. Plant Cell Environ. 4 (5), 391–397. https://doi.org/10.1111/j.1365-3040.1981.tb02117.x.

David, T.S., Pinto, C.A., Nadezhdina, N., Kurz-Besson, C., Henriques, M.O., Quilhó, T., Cermak, J., Chaves, M.M., Pereira, J.S., David, J.S., 2013. Root functioning, tree water use and hydraulic redistribution in Quercus suber trees: a modeling approach based on root sap flow. For. Ecol. Manage. 307, 136–146. https://doi.org/10.1016/j.foreco.2013.07.012.

Granier, A., 1987. Evaluation of transpiration in a douglas-fir stand by means of sap flow measurements. Tree Physiol. 3 (4), 309–319. https://doi.org/10.1093/treephys/3.4.309.

Green, S., Clothier, B., Jardine, B., 2003. Theory and practical application of heat pulse to measure sap flow. Agron. J. 95 (6), 1371–1379. https://doi.org/10.2134/agronj2003.1371.

Kluitenberg, G.J., Ham, J.M., 2004. Improved theory for calculating sap flow with the heat pulse method. Agric. For. Meteorol. 126 (1–2), 169–173. https://doi.org/10.1016/j.agrformet.2004.05.008.

Kluitenberg, G.J., Das, B.S., Bristow, K.L., 1995. Error analysis of heat pulse method for measuring soil heat capacity, diffusivity, and conductivity. Soil Sci. Soc. Am. J. 59 (3), 719–726. https://doi.org/10.2136/sssaj1995.03615995005900030013x.

Lu, P., Urban, L., Zhao, P., 2004. Granier's thermal dissipation probe (TDP) method for measuring sap flow in trees: theory and practice. Acta Bot. Sin.—Engl. Ed. 46 (6), 631–646.

Marshall, D.C., 1958. Measurement of sap flow in conifers by heat transport. Plant. Physiol. 33 (6), 385–396. http://www.plantphysiol.org/content/plantphysiol/33/6/385.full.pdf.

Nybo, E., et al., 2018. Flow velocity maps measured by nuclear magnetic resonance in medical intravenous catheter needleless connectors. J. Pharm. Biomed. 152, 1–11. https://www.researchgate.net/publication/263543943_lu-2004_ABS-Corrected_for_WEbimage.

Peng, X.P., Fan, J., Wang, Q.J., Warrington, D., 2015. Discrepancy of sap flow in Salix matsudana grown under different soil textures in the water-wind erosion crisscross region on the Loess Plateau. Plant Soil 390 (1–2), 383–399. https://doi.org/10.1007/s11104-014-2333-0.

Ren, T., Kluitenberg, G.J., Horton, R., 2000. Determining soil water flux and pore water velocity by a heat pulse technique. Soil Sci. Soc. Am. J. 64 (2), 552–560. https://doi.org/10.2136/sssaj2000.642552x.

Schaeffer, S.M., Williams, D.G., Goodrich, D.C., 2000. Transpiration of cottonwood/willow forest estimated from sap flux. Agric. For. Meteorol. 105 (1–3), 257–270. https://doi.org/10.1016/S0168-1923(00)00186-6.

Sheng, W.Y., Rumana, K., Sakai, M., Silfa, F., Jones, S.B., 2016. A multi-functional penta-needle thermo-dielectric sensor for porous media sensing. IEEE Sens. J. 16 (10), 3670–3678. https://ieeexplore.ieee.org/iel7/7361/4427201/07400927.pdf.

Steinhagen, H.P., 1977. Thermal Conductive Properties of Wood, Green or Dry, from −40° to +100 °C. USDA Forest Service General Technical Report FPL-9. . https://www.fpl.fs.fed.us/documnts/fplgtr/fplgtr09.pdf.

Steppe, K., De Pauw, D.J.W., Doody, T.M., Teskey, R.O., 2010. A comparison of sap flux density using thermal dissipation, heat pulse velocity and heat field deformation methods. Agric. For. Meteorol. 150 (7–8), 1046–1056. https://doi.org/10.1016/j.agrformet.2010.04.004.

Swanson, R., 1983. Numerical and Experimental Analyses of Implanted-Probe Heat Pulse Velocity Theory. PhD Thesis. University of Alberta, Edmonton, Canada.

Swanson, R.H., Whitfield, D.W.A., 1981. A numerical-analysis of heat pulse velocity theory and practice. J. Exp. Bot. 32 (126), 221–239. https://doi.org/10.1093/jxb/32.1.221.

Vandegehuchte, M.W., Steppe, K., 2012a. Improving sap flux density measurements by correctly determining thermal diffusivity, differentiating between bound and unbound water. Tree Physiol. 32 (7), 930–942. https://doi.org/10.1093/treephys/tps034.

Vandegehuchte, M.W., Steppe, K., 2012b. Interpreting the heat Field deformation method: erroneous use of thermal diffusivity and improved correlation between temperature ratio and sap flux density. Agric. For. Meteorol. 162, 91–97. https://doi.org/10.1016/j.agrformet.2012.04.013.

Vandegehuchte, M.W., Steppe, K., 2012c. Sapflow+: a four-needle heat-pulse sap flow sensor enabling nonempirical sap flux density and water content measurements. New Phytol. 196 (1), 306–317. https://doi.org/10.1111/j.1469-8137.2012.04237.x.

Vandegehuchte, M.W., Steppe, K., 2012d. Use of the correct heat conduction-convection equation as basis for heat-pulse sap flow methods in anisotropic wood. J. Exp. Bot. 63 (8), 2833–2839. https://doi.org/10.1093/jxb/ers041.

Vertessy, R.A., Hatton, T.J., Reece, P., OSullivan, S.K., Benyon, R.G., 1997. Estimating stand water use of large mountain ash trees and validation of the sap flow measurement technique. Tree Physiol. 17 (12), 747–756. https://doi.org/10.1093/treephys/17.12.747.

Yang, C.B., Jones, S.B., 2009. INV-WATFLX, a code for simultaneous estimation of soil properties and planar vector water flux from fully or partly functioning needles of a penta-needle heat-pulse probe. Comput. Geosci.—UK 35 (11), 2250–2258. https://doi.org/10.1016/j.cageo.2009.04.005.

Yang, C.B., Sakai, M., Jones, S.B., 2013. Inverse method for simultaneous determination of soil water flux density and thermal properties with a penta-needle heat pulse probe. Water Resour. Res. 49 (9), 5851–5864. https://doi.org/10.1002/wrcr.20459.